Journal of Solid State Chemistry 184 (2011) 863–870

Contents lists available at ScienceDirect

Journal of Solid State Chemistry

journal homepage: www.elsevier.com/locate/jssc

B-site substitutions in $LaNb_{1-x}M_xO_{4-\delta}$ materials in the search for potential proton conductors (M=Ga, Ge, Si, B, Ti, Zr, P, Al)

A.D. Brandão [a], J. Gracio [b], G.C. Mather [c], V.V. Kharton [a], D.P. Fagg [b,*]

[a] Dept. Ceramics and Glass Engineering, CICECO, University of Aveiro, 3810-193 Aveiro, Portugal
[b] Nanotechnology Research Division, Centre of Mechanical Technology and Automation, University of Aveiro, 3810 193 Aveiro, Portugal
[c] Institute of Ceramics and Glass, CSIC, Cantoblanco, 28049 Madrid, Spain

ARTICLE INFO

Article history:
Received 15 October 2010
Received in revised form
18 January 2011
Accepted 11 February 2011
Available online 19 February 2011

Keywords:
Ceramic Proton conductor
Solid oxide fuel cell
$LaNbO_4$
Scheelite
Fergusonite
Electrolyte
Solid solubility

ABSTRACT

The solid solubilities of potential B-site dopants in $LaNb_{1-x}M_xO_{4-\delta}$, materials, M=Ga, Ge, Si, Al, B, P, Zr or Ti, have been investigated in the search for possible novel proton conductors. In general, the solubility levels of these cations were found to be very low ($x \leq 0.03$). At the maximum value x=0.03, only compositions containing Ti, Ge, Ga and Si appeared pure at the limit of resolution of XRD. The literature phase diagram, La_2O_3–Nb_2O_5–ZrO_2, has been re-analysed for compositions of low Zr-content around the composition $LaNbO_4$. The electrical properties of phase pure Ti-doped compositions have been studied. Higher bulk and total conductivities were observed in wet than dry conditions, suggesting a significant protonic contribution to total conductivity. In wet conditions, the activation energy for bulk conductivity of $LaNb_{0.98}Ti_{0.02}O_{4-\delta}$ was found to be much higher than that of an A-site, Sr-doped material, $Sr_{0.02}La_{0.98}NbO_{4-\delta}$, of similar acceptor dopant concentration. The Sr-doped composition offered higher conductivities than the Ti-doped composition up to approximately 900°C.

1. Introduction

The most common ceramic-oxide, proton-conducting materials are those based on perovskite oxides (ABO_3) containing large basic A cations (e.g. Ba, Sr) and tetravalent B cations (e.g. Zr, Ce). In the case of the cerates, the basicity of the A cation leads to poor tolerance to CO_2, rapidly decomposing to form the carbonates at higher temperatures [1,2]. This is a major problem when one considers using these materials in devices such as fuel cells or hydrogen-separation membranes that operate in hydrocarbon environments. Recently, alternative proton-conducting materials have been suggested that offer high CO_2 tolerances, such as systems based on the fergusonite/scheelite ABO_4 structure types [3–7]. The characterisation of these phases is still in its infancy, with most work being performed by Haugsrud et al. [3–6]. The highest proton conductivity recorded so far is the material $LaNbO_4$ when it contains minor A-site acceptor substitutions, such as $Ca_{0.01}La_{0.99}NbO_{4-\delta}$. Nonetheless, peak conductivity values currently remain an order of magnitude lower than those attainable in the best perovskite proton conductors. Despite this limitation, the purity of proton conduction in this class of materials has led to suggested application as hydrogen and humidity sensors at temperatures below about 700 °C [3].

When doped with acceptor cations to form oxygen vacancies, the ABO_4 compositions incorporate protons in the presence of H_2O, with hydroxyl groups filling the vacancies and protons forming additional hydroxyl groups with lattice oxygens [3–6]. This is an analogous process to proton incorporation in the perovskite materials [1]. Hence, one should note that the oxygen-vacancy concentration in the ABO_4 materials remains approximately ten times less than that of the common perovskite proton conductors due to very low solubilities of A-site acceptor dopants in the fergusonite structure (approximately 1–2% of the A-site [3–6]). This factor will lead to a low number of protonic charge carriers and potentially also low levels of conductivity. In this respect it is interesting to note that previous attempts to introduce proton conduction in these materials have solely concentrated on acceptor doping on the A-site [3–6]. Nevertheless, one can also create oxygen vacancies as charge-compensating defects by acceptor doping on the B-site. Hence, the current article assesses this possibility, providing information on the level of solubility of B-site acceptor dopants and their impact on transport properties in these ABO_4 materials in the search for novel proton conductors offering higher conductivity.

Furthermore, recent work by the current authors [7] demonstrated that the introduction of a smaller, isovalent, cation on the B-site of these ABO_4 compositions (vanadium) stabilised the scheelite phase to room temperature, in agreement with predictions of Bastide [8] and Manjón et al. [9] based on cation–anion radii ratios and ABO_4 coordination chemistry. This strategy

* Corresponding author.
E-mail address: duncan@ua.pt (D.P. Fagg).

0022-4596/$ - see front matter © 2011 Elsevier Inc. All rights reserved.
doi:10.1016/j.jssc.2011.02.012

successfully avoided the fergusonite/scheelite phase transformation, eliminating the characteristic break in TEC coefficient that may otherwise be problematic for application of $LaNbO_4$-based materials as proton-conducting electrolytes. In addition, the high temperature scheelite phase exhibits a lower activation energy for proton conduction, in comparison to a rapid decay of conductivity with decreasing temperature for the fergusonite polymorph [3,7]. Hence, retention of the high temperature scheelite phase to room temperature by doping with smaller B-site cations can also, potentially, lead to preservation of high levels of proton conductivity to lower temperatures [7].

The B-site elements studied in this work are the following aliovalent dopants, Ga, Ge, Si, B, Ti, Zr, Al, and also the isovalent dopant, P. These dopants, therefore, encompass cations that are smaller and also larger than the host cation, while the aliovalent group also serves to introduce oxygen vacancies as charge-compensating defects. As potential B-site acceptor substitutions have not previously been attempted experimentally in this class of material, this preliminary work is expected to encourage many further studies.

2. Experimental

2.1. Sample preparation and materials properties

Powders of $LaNb_{1-x}M_xO_{4-\delta}$ were prepared by solid-state synthesis starting from stoichometric mixtures of La_2O_3 (Aldrich, 99.99%), Nb_2O_5 (Merck, 99%), with Ga_2O_3 (Aldrich, 99.99%), GeO_2 (Aldrich, 99.998%), SiO_2 (Thiokol, 99.9%), TiO_2 (Aldrich, 99.8%), ZrO_2 (Aldrich, 99%), Al_2O_3 (Sigma-Aldrich, 99.7%), H_3BO_3 (Merck) or $(NH_4)H_2PO_4$ (Sigma-Aldrich, 99.999%). Prior to weighing, the La_2O_3 and Ga_2O_3 powders were calcined at 700 °C for 1 h. Stoichiometric amounts of the reagents were intimately mixed in a pestle and mortar under acetone and uniaxially dry pressed into pellets at a pressure of 30 MPa. The samples $LaNb_{1-x}M_xO_{4-\delta}$, M= Ti, Zr and Al were fired at 1500 °C for 10 h, while the samples for M=Ga, Ge, Si, B and P were sintered at 1300 °C for 12 h. Phase analysis was performed by X-ray diffraction (XRD), on crushed powders using a Rigaku Geigerflex diffractometer (Cu *K*a radiation), (20–65° 2θ, step 0.02, 1.5°/min).

The samples $LaNb_{1-x}Ti_xO_{4-\delta}$, x=0.02 and 0.03 had densities exceeding 90% of the theoretical density. Average grain sizes were calculated to be in the range of 5–10 μm for the $LaNb_{0.98}Ti_{0.02}O_{4-\delta}$ and $LaNb_{0.97}Ti_{0.03}O_{4-\delta}$ materials from SEM images, using the image processing programme Image J 1.37v software (Wayne Rasband, National Institutes of Health, USA). Thermal-expansion behaviour was followed using a Linseis dilatometer on rectangular green compacts ($1.4 \times 0.5 \times 0.3$ cm^3) with a constant heating and cooling rate of 10 °C/min.

2.2. Electrical measurements

Impedance spectroscopy was performed using an Electrochemie-Autolab PGSTAT302N analyser in the frequency range 1 MHz–0.01 Hz, amplitude 50 mV, on dense pellets, approximately 3 mm × 8 mm diameter, painted with two porous platinum electrodes, in an isolated chamber under both wet and dry nitrogen and oxygen atmospheres, with a flow rate 50 ml/min. The impedance data were de-convoluted to obtain contributions ascribed to bulk, grain boundaries and external interfaces, as suggested by typical capacitance values in the ranges of 10–20 pF/cm^2, about 1 nF/cm^2, and about 1 μF/cm^2, respectively [10]. Measurements were made at 50 °C intervals in the direction of decreasing temperature. Stability was confirmed by performing repeated impedance measurements at each temperature. Humidification was obtained by bubbling gases through water followed by a saturated KCl solution in contact with solid KCl, producing approximately 86% relative humidity at room temperature. Drying was carried out by passing gases through a Varian moisture gas clean filter.

The total specific conductivity of the grain boundaries in series with the bulk material can be estimated using the brick-layer model as [11]

$$\sigma_{g.b} = \frac{L}{A}\left(\frac{C_{bulk}}{C_{g.b.}}\right)\frac{1}{R_{g.b.}} \quad (1)$$

where A is the cross-sectional area, L is the length, $R_{g.b.}$ is the grain boundary resistance extracted from the impedance spectra, and C_{bulk} and $C_{g.b.}$ are the bulk and boundary capacitances, respectively.

Activation energies (E_a) for the bulk and specific grain-boundary conductivities were calculated by the standard Arrhenius equation where A_o is the pre-exponential factor

$$\sigma = \frac{A_o}{T}\exp\left[-\frac{E_a}{RT}\right] \quad (2)$$

3. Results and discussion

3.1. Phase purity. $LaNb_{1-x}M_xO_{4-\delta}$

3.1.1. Dopant M=Ga, Ge, Si, B, Al, P

Despite repeated cycles of high-temperature firing and regrinding (1300 °C for 12 h), phase purity was not obtained for Ga, Ge, Si, B dopants by the solid-state preparation technique at the dopant level of x=0.05. The phases present in the X-ray powder diffraction patterns for dopants Ge and Si, were that of a phase isostructrual with $La_{0.33}NbO_3$, JCPDS No. 01-070-6201, in addition to that of the main fergusonite phase. In contrast, the formation of $LaBO_3$, JCPDS No. 00-012-0762, and $LaGaO_3$, JCPDS No. 01-081-2302, as secondary phases can be observed in the B- and Ga-doped samples, respectively, Fig. 1. At the lower dopant concentration of x=0.03, compositions substituted with Ge, Ga and Si appear pure at the resolution limit of XRD, while for the B-case, the secondary phase $LaBO_3$ persists. The lattice constants for the Ga-, Ge-, and Si-doped compositions are presented in Table 1. As many of these dopants are volatile, further study at higher temperatures was not performed. In contrast, further analysis was performed at 1500 °C for the system containing Al. In spite of this increase in temperature, an impurity phase of $LaAlO_3$, JCPDS No. 01-70-4113 remains at the dopant level x=0.03, Fig. 2.

In the case of isovalent P-doping, one aimed to maintain the high-temperature scheelite phase to lower temperature by the introduction of a smaller B-site dopant [7–9,12]. Note that in the analogous case of $LaNb_{1-x}V_xO_4$, this required quite high dopant levels of between x=0.2 and x=0.37 [12]. Unfortunately, in contrast to vanadium, the phosphorous doped system shows very poor solubility in the $LaNbO_4$ structure. The impurity phases $LaPO_4$ (JCPDS No. 01-071-6745) and Nb_2O_5 (JCPDS No. 01-071-0336) are observed for the P-doped system, sintered at 1300 °C for 12 h, even at low dopant levels, Fig. 3.

3.1.2. Dopant M=Zr

The phase diagram of the system La_2O_3–Nb_2O_5–ZrO_2 published by Zheng and West [13] suggests solubility of Zr in $LaNb_{1-x}Zr_xO_{4-\delta}$ up to values of approximately x=0.05 at 1500 °C. Unfortunately, on preparation of this composition and also compositions of lower x values, down to x=0.02, phase purity was not obtained by solid-state synthesis even after many cycles of high-temperature firing and regrinding. The impurity phase $La_2Zr_2O_7$ remained in addition to the main fergusonite phase. This is perhaps to be expected as the phase diagram of Zheng et al. does not contain many data points in the

current area of interest. Hence, to verify the true solubility limit of Zr in $LaNbO_4$, several additional compositions were prepared to extend the phase regions suggested by Zheng et al. with higher precision in the vicinity of composition $LaNbO_4$, Fig. 4. Note that the limit of resolution of secondary phases on the binary joins $La_2Zr_2O_7$–$LaNbO_4$ and ZrO_2–$LaNbO_4$ was tested experimentally by powder X-ray diffraction to be 0.5% and 1%, respectively, i.e. safely below that of the studied compositions. Fig. 4 shows the $LaNbO_4$ solid solution to be much smaller than that suggested in the diagram of Zheng et al. For example, on the $LaNb_{1-x}Zr_xO_4$ join, the solid solution limit is below that of $x=0.02$. Unfortunately, this low level of solubility would not offer significant benefit over the solubility limits of current A-site dopants; hence, further work on this system was discontinued.

3.1.3. Dopant M=Ti

At 1300 °C no solid solubility of Ti in $LaNbO_4$ is observed. However, at 1500 °C the XRD patterns exhibit the pure fergusonite phase for compositions $x=0.02$ and 0.03, whereas a secondary phase of $La_2Ti_2O_7$ can be observed for the composition $x=0.05$, Fig. 5. At such high sintering temperatures, one should take care with subsequent analysis as the eutectic temperature of the pseudo-binary join $LaNbO_4$–$La_2Ti_2O_7$ is documented by Udalov et al. [14] to occur at 1580 °C in comparison to only 1480 °C for the pseudo-binary join $LaNbO_4$–TiO_2. Hence, it is

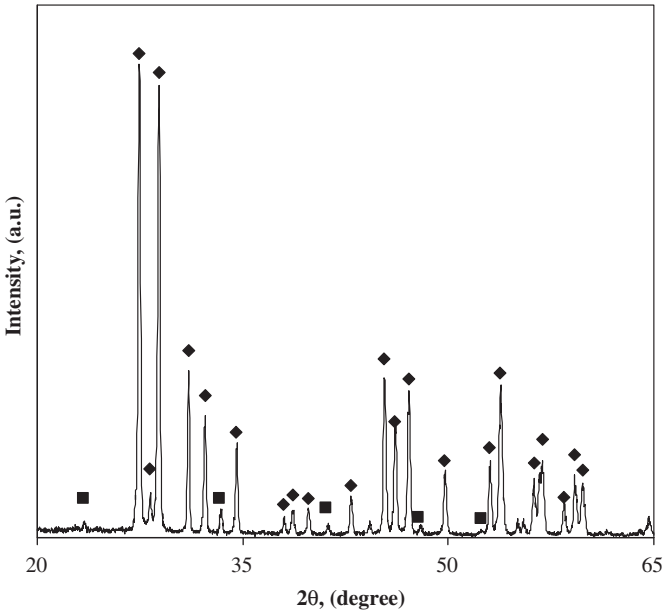

Fig. 2. XRD pattern of $LaNb_{0.97}Al_{0.03}O_{4-\delta}$ material. The markers identify (♦) the $LaNbO_4$ fergusonite phase and (■) the $LaAlO_3$ phase.

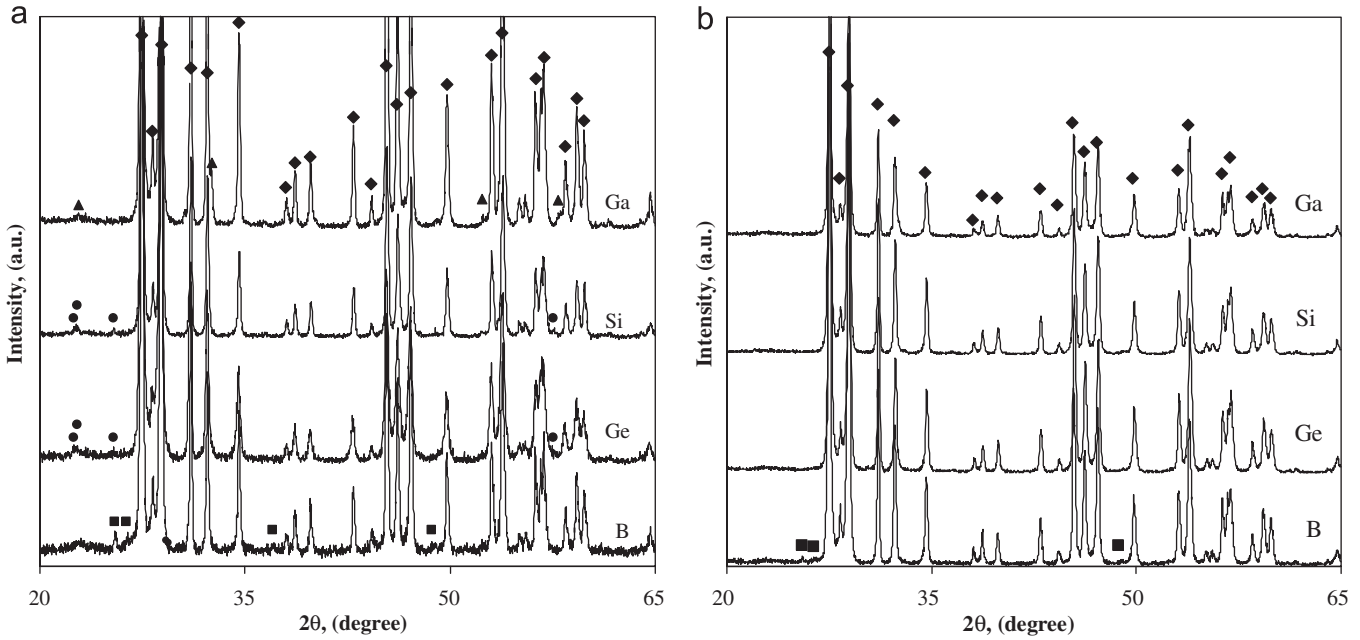

Fig. 1. XRD patterns of $LaNb_{1-x}M_xO_{4-\delta}$ materials, M=B, Ge, Si and Ga, for (a) $x=0.05$ and (b) $x=0.03$. The markers identify (♦) the $LaNbO_4$ fergusonite phase, (■) the $LaBO_3$ phase, (●) the $La_{0.333}NbO_3$ phase and (▲) the $LaGaO_3$ phase.

Table 1
Lattice constants of $LaNb_{1-x}M_xO_{4-\delta}$ compounds, M=Ga, Ti, Ge, Si.

	Composition x	a, (Å) ± 0.0005	b, (Å) ± 0.0008	c, (Å) ± 0.0004	β, (deg.) ± 0.004	V, (Å^3) ± 0.05
	0	5.5667(2)[a]	11.5245(4)[a]	5.2002(3)[a]	94.084(2)[a]	332.88(4)[a]
Ga	0.03	5.5569(3)	11.5145(8)	5.1980(3)	94.048(3)	331.76(4)
	0.05	5.5570(3)	11.5093(6)	5.1961(3)	94.075(3)	331.49(3)
Ti	0.02	5.5591(5)	11.5135(8)	5.1987(4)	94.067(4)	331.91(5)
	0.03	5.5586(2)	11.5104(5)	5.1970(2)	94.084(2)	331.67(2)
	0.05	5.5585(3)	11.5091(6)	5.1976(3)	94.076(3)	331.66(3)
Ge	0.03	5.5570(3)	11.5141(6)	5.1977(3)	94.0257(3)	331.73(3)
	0.05	5.5580(3)	11.5150(7)	5.1981(3)	94.029(3)	331.85(3)
Si	0.03	5.5566(3)	11.5119(6)	5.1970(3)	94.049(3)	331.61(3)
	0.05	5.5579(3)	11.5117(6)	5.1971(3)	94.065(3)	331.68(3)

[a] Values from Ref. [12]

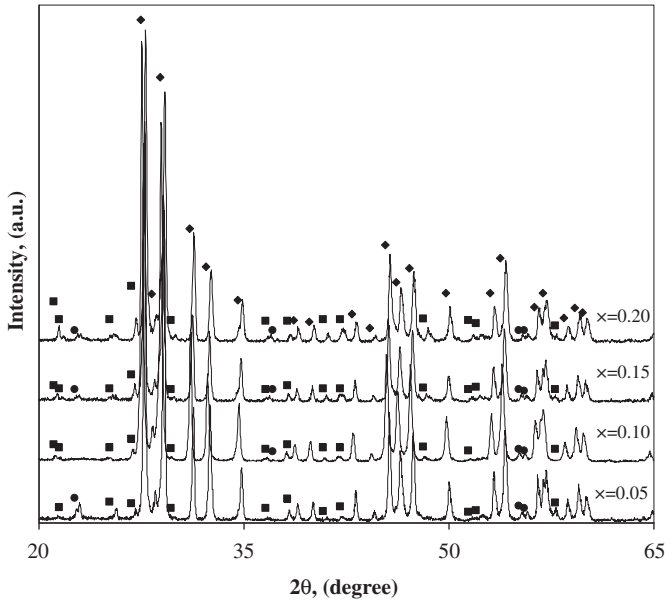

Fig. 3. XRD patterns of $LaNb_{1-x}P_xO_{4-\delta}$ materials for values of $x=0.05$, 0.10, 0.15 and 0.20. The markers identify (♦) the $LaNbO_4$ fergusonite phase, (■) the $LaPO_4$ monazite phase and (●) the Nb_2O_5 phase.

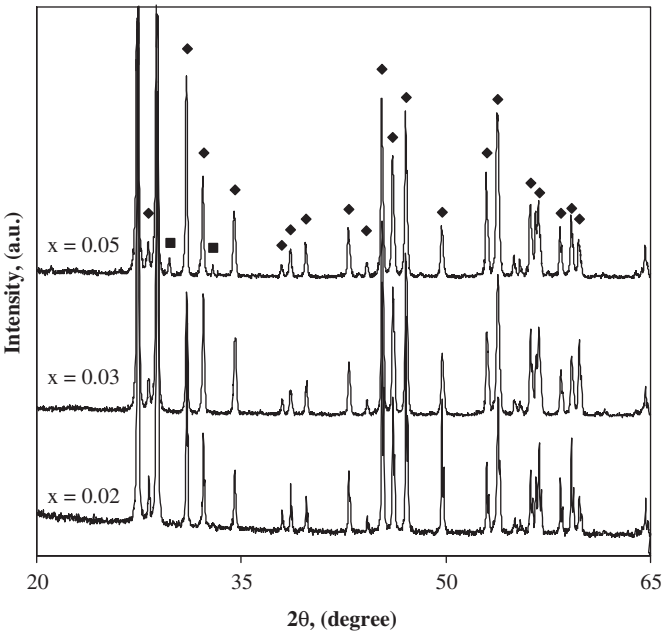

Fig. 5. XRD patterns of $LaNb_{(1-x)}Ti_xO_{4-\delta}$ materials for $x=0.02$, $x=0.03$ and $x=0.05$. The markers identify (♦) the $LaNbO_4$ fergusonite phase and (■) identify the $La_2Ti_2O_7$ phase.

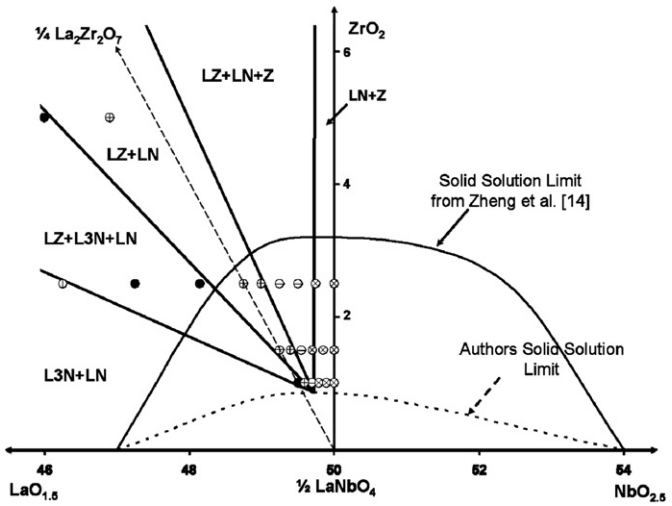

Fig. 4. Phase diagram of the system La_2O_3–Nb_2O_5–ZrO_2. The data points represent the compositions studied in this work, where (ⓘ) identifies the presence of the two phases of La_3NbO_7 (L3N) and $LaNbO_4$ (LN), (●) identifies the phases $La_2Zr_2O_7$ (LZ), La_3NbO_7 and $LaNbO_4$, (⊕) identifies the phases $La_2Zr_2O_7$ and $LaNbO_4$, (⊖) identifies the three phases of $La_2Zr_2O_7$, $LaNbO_4$ and ZrO_2 (Z), and (⊗) identifies the presence of the phases $LaNbO_4$ and ZrO_2 (Z).

important to eliminate any possibility that an amorphous, liquid phase forms as a result of compositional inhomogenity (especially in compositions of low Ti-content, due to close proximity of these two joins) as such a phenomenon would lead to an apparently pure XRD-pattern but a false conclusion of Ti solid solubility. Fig. 6 shows SEM micrographs of the composition $LaNb_{0.98}Ti_{0.02}O_{4-\delta}$ (join $LaNbO_4$–$La_2Ti_2O_7$) compared to that of $La_{0.99}Nb_{0.99}Ti_{0.02}O_{4-\delta}$ (join $LaNbO_4$–TiO_2). The intended composition, $LaNb_{0.98}Ti_{0.02}O_{4-\delta}$, is shown to be free from liquid phases suggesting true solid solubility of Ti in the B-site of $LaNb_{1-x}Ti_xO_4$, in stark contrast to the La-deficient composition, $La_{0.99}Nb_{0.99}Ti_{0.02}O_{4-\delta}$, from the $LaNbO_4$–TiO_2 join. Hence, this experiment proves categorically that the adopted preparation route offers a high level of stoichiometric

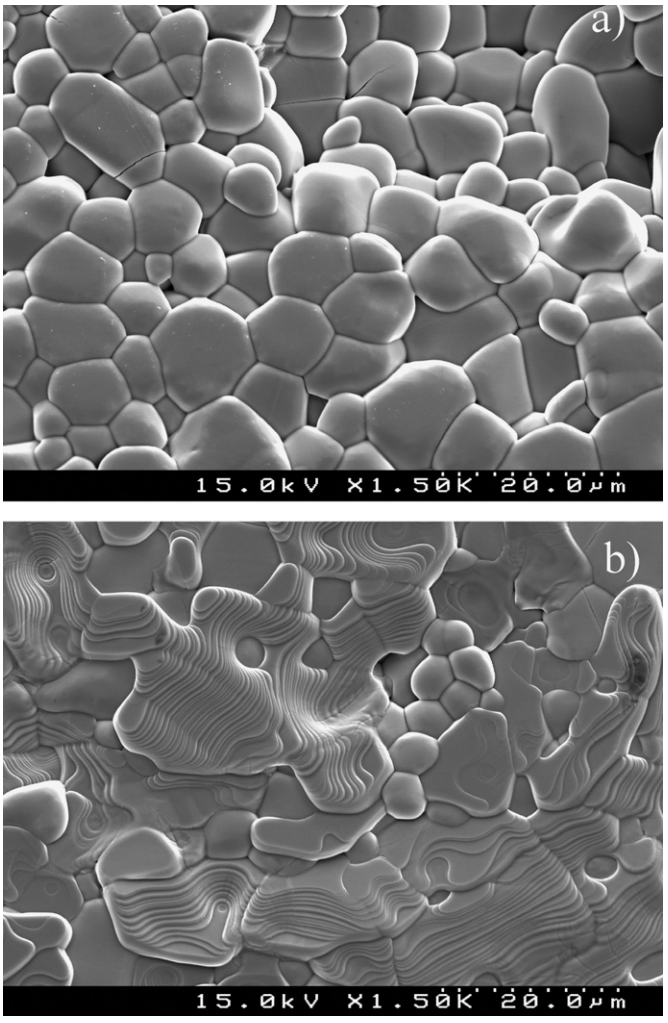

Fig. 6. SEM micrographs of the compositions a) $LaNb_{0.98}Ti_{0.02}O_{4-\delta}$ (join $LaNbO_4$–$La_2Ti_2O_7$) and b) $La_{0.99}Nb_{0.99}Ti_{0.02}O_{4-\delta}$ (join $LaNbO_4$–TiO_2).

accuracy. Further evidence for solid solubility of Ti in $LaNbO_4$ is given by the lower lattice volume for the Ti-containing compositions, Table 1, related to the smaller ionic radius of Ti in comparison to Nb. Unambiguous evidence is, therefore, provided of solid solubility of Ti in $LaNbO_4$, allowing the properties of compositions on the $LaNb_{1-x}Ti_xO_{4-\delta}$ join to be assessed further. However, the similar lattice volumes recorded for compositions $x=0.02$ and $x=0.03$, suggest that the true solid solubility limit may lie closer to composition $x=0.02$.

3.1.4. Phase purity discussion

A very recent atomistic simulation study by Mather et al. [15] offers predictions for the solubility of acceptor dopants in $LaNbO_4$ materials. This work suggested unfavourable solution energies for dopants with a large mismatch of ionic radius with the Nb host (such as Ge), but improved solubilities for Ti and Zr with a closer match in ionic radii. In this respect, the lower solubility of Zr in $LaNbO_4$, indicated by XRD in Section 3.1.2, in comparison to the smaller ions, Ga, Ge and Si, appears to be in direct contradiction to the simulation [15]. To discuss this further, one should first clarify the equations related to impurity formation for each dopant.

For the 4+ dopants Ge and Si, the observed impurity is isostructural to $La_{0.33}NbO_3$. However, to form this phase requires the simultaneous formation of a La-rich phase involving the 4+ dopant. As the La_xNbO_3 structure shows some compositional flexibility in the range $0.3<x<0.43$ [13], one can estimate that this La-rich phase should lie in the apatite or two phase apatite+La_2SiO_5/La_2GeO_5 compositional regions [16]. Eq. (3) demonstrates this suggestion for the apatite phase, with an analogous situation proposed for the Ge dopant.

$$LaNb_{1-x}Si_xO_4 \rightarrow x/6La_{10-6y}Si_6O_{26+\delta}+xLa_{0.33+y}NbO_{3+y} + 1-2x\ LaNbO_4 \quad (3)$$

It is clear from Eq. (3) that the relative concentration of apatite-related impurities, would be very low and, hence, perhaps below the limit of resolution of the XRD technique, thus leaving the $La_{0.33}NbO_3$-based phase as the only observable impurity.

Secondary phase formation in the Zr (or analogously the Ti) case is observed to lead to the formation of pyrochlore phases according to

$$LaNb_{1-x}Zr_xO_4 \rightarrow x/2La_2Zr_2O_7+1-xLaNbO_4 \quad (4)$$

while in the case of 3+ dopants (M^{3+}) one generally observes the formation of perovskite impurity phases, $LaMO_3$, such as $LaBO_3$, $LaGaO_3$ and $LaAlO_3$, Section 3.1.1.

$$LaNb_{1-x}M_xO_4 \rightarrow xLaMO_3+1-xLaNbO_4 \quad (5)$$

In quantitative analysis by XRD, the scale factor S of a particular phase accounts for the intensity diffracted by that phase. Following Bish and Howard [17], the weight fraction of the ith component of density ρ_i in a mixture of n phases can be obtained from

$$W_i = S_i\rho_i \Big/ \sum_{j-1}^{n} S_j\rho_j \quad (6)$$

The impurity phases forming in the cases of Eqs. (3) and (4) are, respectively, a $La_{0.33}NbO_3$-based phase ($M=187.21$ g; $\rho=5.13$ g cm^{-3}) and the $La_2Zr_2O_7$ phase ($M=572.26$ g; $\rho=6.02$ g cm^{-3}). If these phases exist in the same molar ratio in any given mixture then the ratio of their scale factors is given by

$$\frac{S_{La_2Zr_2O_2}}{S_{La_{0.33}NbO_3}} = \frac{M_{La_2Zr_2O_7}}{M_{La_{0.33}NbO_3}} \cdot \frac{\rho_{La_{0.33}NbO_3}}{\rho_{La_2Zr_2O_7}} \approx 2.6 \quad (7)$$

Hence, one should be aware that the scale factor of the impurity phase $La_2Zr_2O_7$ will be much higher than that of a $La_{0.33}NbO_3$-based phase for the same molar ratio, rendering its identification much easier by X-ray diffraction. The apparent higher solid solubility noted for compositions $LaNb_{0.97}Si_{0.03}O_{4-\delta}$ and $LaNb_{0.97}Ge_{0.03}O_{4-\delta}$ may, alternatively, therefore, be related to the different limits of resolution of each impurity phase by XRD. In this respect it should be noted that the lattice volumes of these Ga-, Ge- and Si-doped compositions, at the dopant level $x=0.03$, are very similar, despite substantial decreases in ionic radii in the sequence Ga > Ge > Si. A further complication may also manifest itself with respect to assessment of phase purity in the composition $LaNb_{0.95}Ga_{0.05}O_{4-\delta}$, as the main peak of the expected impurity phase, $LaGaO_3$ (1 1 0), coincides with the (2 0 0) reflection of the fergusonite, $LaNbO_4$ phase, rendering its detection more difficult.

Hence, it is clear that further work must be performed to corroborate the apparent phase purity of the Ge, Si, and Ga materials using complimentary techniques, such as Raman, HRTEM or neutron diffraction studies which are beyond the scope of the current article. Nonetheless, the current work show that the solubility of these dopants is expected to be low, $x \leq 0.03$. In the proceeding work, only the $LaNb_{1-x}Ti_xO_{4-\delta}$ system will be studied further to determine thermal-expansion and electrical properties.

3.2. Defect chemistry

Assuming that charge compensation in a generic fergusonite material $LaNb_{1-x}Ti_xO_{4-\delta}$ is exclusively determined by ionic defects, the substitution of Nb for Ti can be described in Kröger–Vink notation as

$$LaO_{1.5}+(1-x)NbO_{2.5}+xTiO_2 \rightarrow La_{La}^{x}+xTi_{Nb}^{/}+(1x)Nb_{Nb}^{x} + 0.5xV_O^{\bullet\bullet}+(4-0.5x)O_O^{x} \quad (8)$$

In a similar way to that described in Refs. [3,7], the equilibrium of oxygen vacancies and electron-holes with the surrounding atmosphere can be described by

$$V_O^{\bullet\bullet}+\frac{1}{2}O_2(g) \overset{K_{ox}}{\Leftrightarrow} O_O^{x}+2h^{\bullet} \quad (9)$$

with mass action constant

$$K_{ox}=\frac{[O_O^{x}]p^2}{[V_O^{\bullet\bullet}]p_{O_2}^{1/2}} \quad (10)$$

While in a competing process, the incorporation of protons by water-vapour uptake can be described as

$$O_O^{x}+V_o^{\bullet\bullet}+H_2O(g) \overset{K}{\Leftrightarrow} 2OH_O^{\bullet} \quad (11)$$

with mass action constant

$$K=\frac{[OH_O^{\bullet}]^2}{[V_O^{\bullet\bullet}][O_O^{x}]pH_2O} \quad (12)$$

The concentration of electrons can be neglected under oxidising conditions thereby the electroneutrality condition can be simplified to

$$p+[OH_O^{\bullet}]+2[V_O^{\bullet\bullet}] \approx \left[Ti_{Nb}^{/}\right] \quad (13)$$

and as the level of acceptor doping is low

$$h^{\bullet}+[OH_O^{\bullet}]+[V_O^{\bullet\bullet}] \ll [O_O^{x}] \approx [O] \quad (14)$$

Thus, on combining Eqs. (10), (12) and (13)

$$\left(K_{ox}^{1/2}[O]^{-1/2}p_{O_2}^{1/4}+K^{1/2}[O]^{1/2}p_{H_2O}^{1/2}\right)[V_O^{\bullet\bullet}]^{1/2}+2[V_O^{\bullet\bullet}] \approx \left[Ti_{Nb}^{/}\right] \quad (15)$$

and hence

$$[V_O^{\bullet\bullet}] = 0.5\left[Ti_{La}^{/}\right]F_{wc}\left\{(1+F_{wc}^{-1})^{1/2}-1\right\}^2 \quad (16)$$

where

$$F_{wc} = \left\{\left(\frac{K_{ox}}{8[O]\left[Ti_{Nb}^{/}\right]}\right)^{1/2} p_{O_2}^{1/4} + \left(\frac{K[O]}{8\left[Ti_{Nb}^{/}\right]}\right)^{1/2} p_{H_2O}^{1/2}\right\}^2 \quad (17)$$

Note that F_{WC} is a function of both partial pressures of oxygen and water vapour and also of the temperature dependence of mass action constants K_{ox} and K. The combination of Eq. (16) with Eqs. (10) and (12) leads to

$$p = \left(\frac{\left[Ti_{Nb}^{/}\right]K_{ox}F_{wc}}{2[O]}\right)^{1/2} p_{O_2}^{1/4}\left\{(F_{wc}^{-1}+1)^{1/2}-1\right\} \quad (18)$$

and

$$[OH_O^{\bullet}] = \left(\frac{K[O]\left[Ti_{Nb}^{/}\right]F_{wc}}{2}\right)^{1/2} (pH_2O)^{1/2}\left\{(F_{wc}^{-1}+1)^{1/2}-1\right\} \quad (19)$$

Under very dry oxidising conditions, one can assume ($K_{ox}^{1/2}p_{O_2}^{1/4} \gg K^{1/2}[O]p_{H_2O}^{1/2}$), yielding the following:

$$p = \frac{K_{ox}p_{O_2}^{1/2}}{4[O]}\left\{\left(1+\frac{8\left[Ti_{Nb}^{/}\right][O]}{K_{ox}p_{O_2}^{1/2}}\right)^{1/2}-1\right\} \quad (20)$$

with limiting regimes for weakly oxidising (Eq. (21)) and strongly oxidising conditions (Eq. (22))

$$p \approx \left(0.5K_{ox}\left[Ti_{Nb}^{/}\right]/[O]\right)^{1/2} p_{O_2}^{1/4} \quad (21)$$

and

$$p \approx \left[Ti_{Nb}^{/}\right] \quad (22)$$

3.3. Conductivity of $LaNb_{1-x}Ti_xO_{4-\delta}$ in wet/dry oxidising atmospheres

3.3.1. Total and bulk conductivity

Under wet inert atmospheres (e.g. wet N_2) one may expect prevailing proton and oxygen vacancy contributions to electrical transport and a negligible p-type contribution, i.e., ($K_{ox}^{1/2}p_{O_2}^{1/4} \ll K^{1/2}[O]p_{H_2O}^{1/2}$). In such a case, one can simplify Eqs. (17) and (19) to yield

$$[OH_O^{\bullet}] = \frac{K[O]p_{H_2O}}{4}\left\{\left(1+\frac{8\left[Ti_{Nb}^{/}\right]}{K[O]p_{H_2O}}\right)^{1/2}-1\right\} \quad (23)$$

Beyond this regime, under more oxidising conditions, one would perhaps predict significant protonic and p-type electronic contributions, as indicated by Eqs. (18) and (19). Fig. 7 compares the bulk to the total (bulk+grain boundary) conductivity of $LaNb_{1x}Ti_xO_{4-\delta}$ for values of $x=0.02$ and 0.03 under nitrogen and oxygen in wet ($p(H_2O) \approx 0.026$ atm) and dry ($p(H_2O) \approx 1\times10^{-5}$ atm) atmospheres. Much higher bulk and total conductivities are observed in wet in comparison to dry conditions for both compositions, suggesting significant protonic contributions to total conductivity. A break occurs in the temperature dependence of both the bulk and the total conductivity behaviour at about 600 °C, which is more obvious in wet conditions. Such a break in conductivity behaviour can be related to the fergusonite–scheelite phase transformation, as occurs for similar acceptor-doped $LaNbO_4$ materials reported by Haugsrud et al. [3–6]. The conductivities measured in wet nitrogen and oxygen

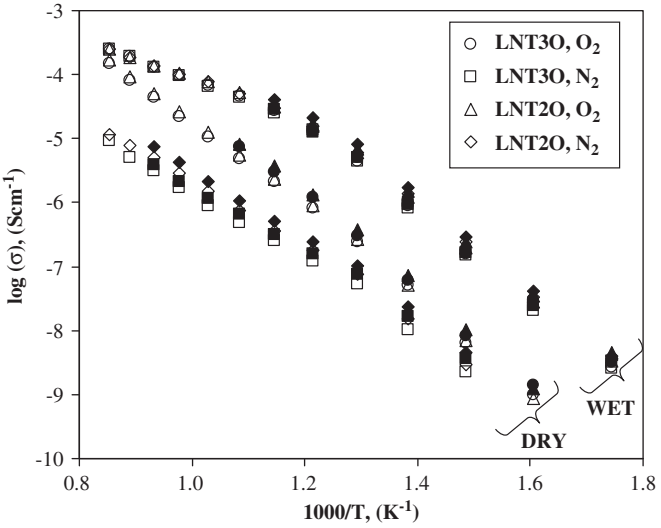

Fig. 7. Total (open symbols) and bulk (closed symbols) conductivities measured in wet ($p(H_2O) \approx 0.026$ atm) and dry ($p(H_2O) \approx 1\times10^{-5}$ atm) nitrogen and oxygen atmospheres for $LaNb_{0.97}Ti_{0.03}O_{4-\delta}$ (LNT3O) and $LaNb_{0.98}Ti_{0.02}O_{4-\delta}$ (LNT2O) materials.

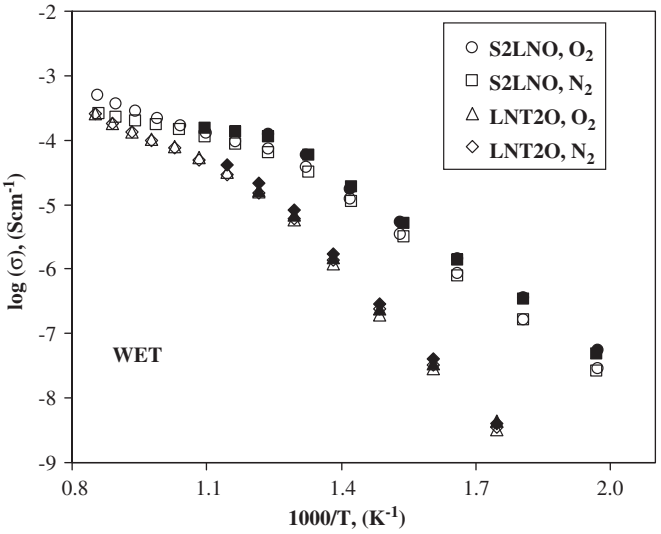

Fig. 8. Comparison of total (open symbols) and bulk (closed symbols) conductivities measured in wet ($p(H_2O) \approx 0.026$ atm) nitrogen and oxygen atmospheres for $LaNb_{0.98}Ti_{0.02}O_{4-\delta}$ (LNT2O) and $Sr_{0.02}La_{0.98}NbO_{4-\delta}$ (S2LNO) materials.

atmospheres mirror each other throughout the examined temperature range, for both compositions, suggesting low levels of p-type conductivity under wet conditions (see Eq. (23)) even for oxidising atmospheres. In contrast, the influence of partial p-type conductivity is revealed in dry conditions with higher conductivities measured in the more oxidising conditions, in agreement with other acceptor-doped $LaNbO_4$ materials [3], and also the related composition $Sr_{0.02}La_{0.98}Nb_{0.7}V_{0.3}O_{4-\delta}$ [7]. Both Ti-containing compositions show slightly higher bulk than total conductivities, suggesting the existence of grain boundary limitations to total conductivity. In general, the conductivities of composition $x=0.02$ are almost equal to that of $x=0.03$. This observation supports the discussion in Section 3.1.3 (based on the similar lattice volumes of these compositions) which placed the limit of solid solution closer to the composition $x=0.02$.

Fig. 8 compares the total and bulk conductivities measured in wet nitrogen and oxygen atmospheres for composition $LaNb_{0.98}Ti_{0.02}O_{4-\delta}$ with that of an A-site, Sr-doped material of

similar acceptor-dopant concentration, $Sr_{0.02}La_{0.98}NbO_{4-\delta}$ [7]. The Sr-doped composition offers substantially higher total and bulk conductivities than the Ti-doped composition throughout the majority of the studied temperature range. Nonetheless, at 900 °C the total conductivity of the Ti-doped composition approaches that of the Sr-doped material. It should be noted that the total conductivity of $Sr_{0.02}La_{0.98}NbO_{4-\delta}$ measured in wet oxygen exceeds that in nitrogen at the highest temperatures, in contrast to the pO_2-independent conductivities noted for the Ti-doped material. This observation can be explained on consideration of the significant p-type electronic contribution of the Sr-doped material as documented in the literature [7]. In comparison to the Sr-doped composition, the Ti-doped composition exhibits a much higher activation energy for conduction (for both the scheelite and fergusonite polymorphs) leading to much more rapid decay of conductivity on decreasing temperature. The bulk activation energies calculated for wet conditions are shown in Table 2. The larger bulk activation energy in the Ti-doped case with respect the A-site Sr-doped composition is in agreement with atomistic simulation studies of Mather et al. [15] who predicted lower dopant-proton trapping energies for acceptor dopants accommodated on the A-site.

3.3.2. *Specific grain-boundary conductivity*

The specific grain-boundary conductivities of $Sr_{0.02}La_{0.98}NbO_{4-\delta}$ are compared to that of $La_{0.98}Nb_{1-x}Ti_xO_{4-\delta}$ in Fig. 9(a) and (b), respectively, for $x=0.02$ and $x=0.03$, measured in various atmospheres. The higher grain-boundary conductivities measured in wet than in dry conditions for all compositions suggest that the grain boundaries of these materials are proton conducting, in agreement with work by Fjeld [18] on the composition $Sr_{0.005}La_{0.995}NbO_{4-\delta}$. The grain-boundary conductivities of the Sr-doped composition are, in general, much higher than the Ti-doped composition. The exception to this trend is at high temperatures in dry oxidising conditions, where the grain boundary conductivity of the Ti-doped compositions exceeds that of the Sr-doped composition. The grain-boundary conductivity in wet conditions is observed to be pO_2 independent for all compositions. In dry conditions the specific grain-boundary conductivity for all compositions decreases on lowering oxygen partial pressure, characteristic of p-type electronic conductivity.

Table 2
Activation energy of the bulk and specific grain boundary conductivity in $Sr_{0.02}La_{0.98}NbO_{4-\delta}$ (S2LNO), $LaNb_{0.98}Ti_{0.02}O_{4-\delta}$ LNT2O) and $LaNb_{0.97}Ti_{0.03}O_{4-\delta}$ (LNT3O) materials in wet conditions, calculated for temperatures below that of the fergusonite–scheelite phase transformation.

	Atmosphere	Composition		
		LNT3O (kJ mol^{-1})	LNT2O (kJ mol^{-1})	S2LNO (kJ mol^{-1})
bulk	O_2	143.5 ± 2	139.0 ± 0 3	92.7 ± 6
bulk	N_2	147.8 ± 3	144.0 ± 2	91.7 ± 3
g.b.	O_2	156 ± 3	134.3 ± 5	92.2 ± 5
g.b.	N_2	148.8 ± 6	137.0 ± 5	94.2 ± 2

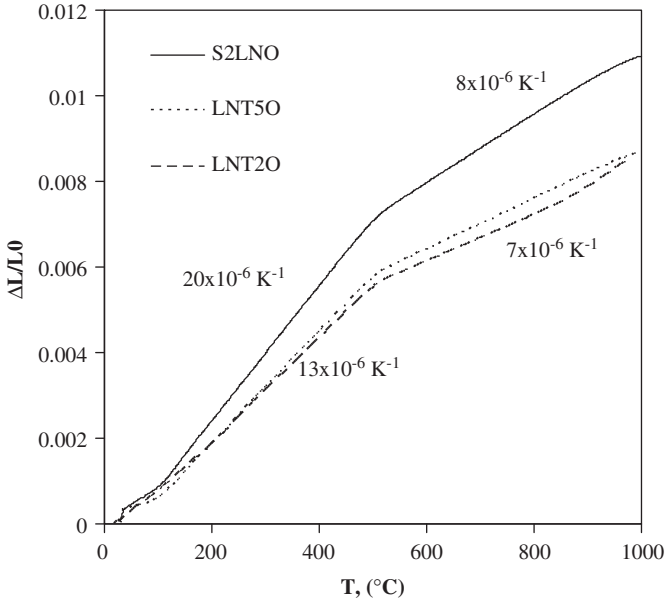

Fig. 10. Thermal expansion behaviour of compositions $LaNb_{0.98}Ti_{0.02}O_{4-\delta}$ LNT2O) and $LaNb_{0.95}Ti_{0.05}O_{4-\delta}$ (LNT5O) compared to that of $Sr_{0.02}La_{0.98}NbO_{4-\delta}$ S2LNO).

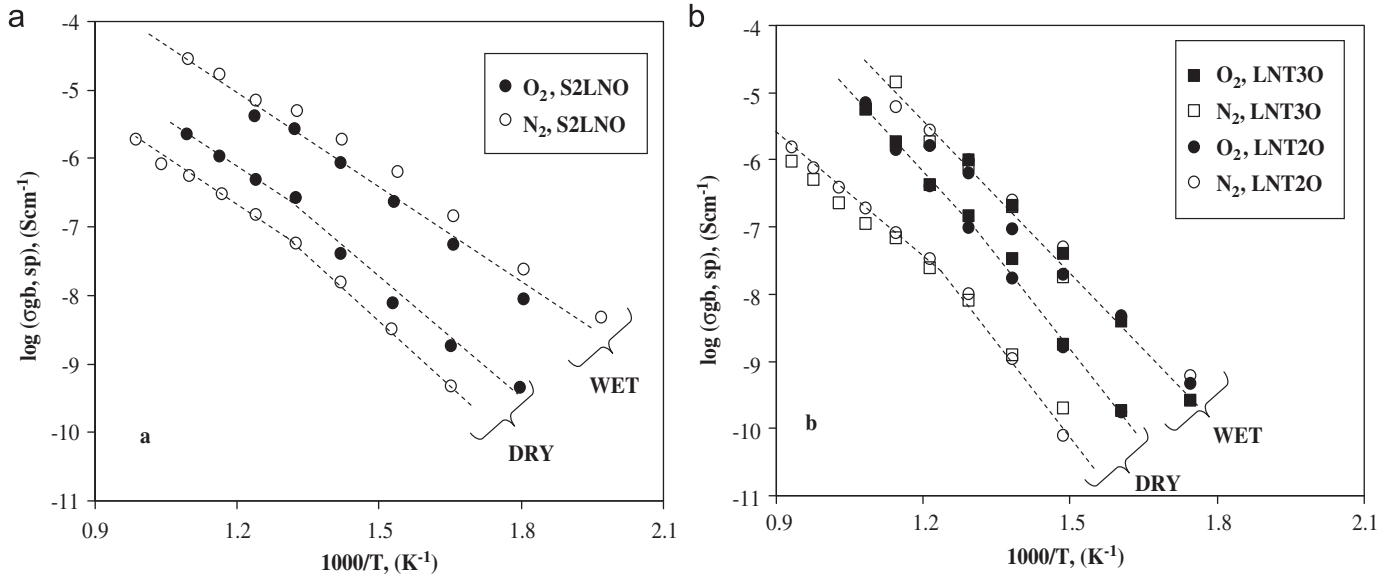

Fig. 9. Comparison of specific grain-boundary conductivities of (a) $Sr_{0.02}La_{0.98}NbO_{4-\delta}$ (S2LNO) with (b) $LaNb_{0.98}Ti_{0.02}O_{4-\delta}$ (LNT2O) and $LaNb_{0.97}Ti_{0.03}O_{4-\delta}$ (LNT3O) materials, measured in wet ($p(H_2O) \approx 0.026$ atm) and dry ($p(H_2O) \approx 1 \times 10^{-5}$ atm) nitrogen and oxygen atmospheres.

The activation energy for grain-boundary conductivity of the Ti-doped materials is much higher than that of the Sr-doped material in all conditions, (activation energies for wet conditions shown in Table 1). Hence, the lower dopant-proton trapping for acceptor dopants accommodated on the A-site in the grain bulk, predicted in the simulation study of Mather et al. [15], may also apply to the grain-boundary behaviour.

3.4. Thermal expansion, $LaNb_{1-x}Ti_xO_{4-\delta}$

Fig. 10 shows the thermal-expansion behaviour of the compositions $LaNb_{1-x}Ti_xO_{4-\delta}$ for $x=0.03$ and $x=0.05$ compared to that of $Sr_{0.02}La_{0.98}NbO_{4-\delta}$. The thermal expansion of all compositions shows clear discontinuities at around 550 °C characteristic of the second-order fergusonite to scheelite phase transformation [3–6]. The respective thermal expansion coefficients (TECs) for the two ranges in the Sr-doped composition are calculated as $20\times10^{-6}\,K^{-1}$ and $8\times10^{-6}\,K^{-1}$. These values are in agreement with literature values for this composition [19]. In contrast, the Ti-doped compositions show lower thermal expansion coefficients than the Sr-doped composition with TEC values of $13\times10^{-6}\,K^{-1}$ and $7\times10^{-6}\,K^{-1}$ for the fergusonite and scheelite structural polymorphs, respectively. Similar TEC values are observed for the two Ti-contents studied, in accordance with the observation made in Section 3.1.3 that the composition $x=0.05$ is beyond the solid-solution limit.

4. Conclusions

A wide range of potential B-site dopants, Ga, Ge, Si, Al, B, P, Zr and Ti, have been investigated with respect to their solubilities in $LaNbO_4$ in the search for possible novel proton conductors. In general, solubility levels were found to be very low. At the dopant level of $x=0.05$, none of the examined dopants were completely soluble in $LaNbO_4$. The observed secondary phases were $La_{0.333}NbO_3$-based for Ge and Si dopants, $LaPO_4$ for the P dopant, $LaGaO_3$, $LaBO_3$ and $LaAlO_3$ for Ga, B and Al dopants, and $La_2Zr_2O_7$ and $LaTi_2O_7$ for Zr and Ti dopants, respectively. At the lower dopant concentration of $x=0.03$, compositions doped with Ti, Ge, Ga and Si appear pure at the resolution limit of XRD. The phase diagram, La_2O_3–Nb_2O_5–ZrO_2, of Zheng et al. [13] has been corrected for compositions of low Zr-content around the composition $LaNbO_4$. The solubility of Zr in $LaNbO_4$ was demonstrated to be much lower than the diagram of Zheng et al. with solubility levels $x<0.02$.

The electrical properties of Ti-doped compositions were studied for the dopant levels $x=0.02$ and $x=0.03$. In dry conditions higher conductivities are measured in more oxidising conditions suggesting a p-type conductivity contribution. Much higher bulk and total conductivities were observed in wet than dry conditions, indicating significant protonic contribution to total conductivity. Slightly higher bulk than total conductivities suggests the existence of grain-boundary limitations to total conductivity in the Ti-doped materials. Nonetheless, the grain boundary is shown to be proton conducting. Comparison of the conductivity behaviour of $LaNb_{0.98}Ti_{0.02}O_{4-\delta}$ to that of an A-site, Sr-doped material of similar acceptor-dopant concentration, $Sr_{0.02}La_{0.98}NbO_{4-\delta}$, shows the Ti-doped composition to exhibit much higher activation energies for conduction in wet conditions, for both the fergusonite and scheelite structural polymorphs. The Sr-doped composition offers higher conductivities than the Ti-doped composition over almost all the studied temperature range.

Acknowledgments

This work was supported by the FCT, Portugal (Grants PTDC/CTM/64357/2006, FCT, SFRH/BD/60265/2009, FCT, PTDC/CTM/105424/2008, PTDC/CTM/100412/2008).

References

[1] K.D. Kreuer, et al., Solid State Ionics 145 (1–4) (2001) 295.
[2] N. Zakowsky, S. Williamson, J.T.S. Irvine, Solid State Ionics 176 (2005) 3019.
[3] R. Haugsrud, T. Norby, Nat. Mater. 5 (2006) 193.
[4] R. Haugsrud, T. Norby, Solid State Ionics 177 (2006) 1129.
[5] R. Haugsrud, B. Ballesteros, M. Lira-Cantú, T. Norby, J. Electrochem. Soc. 153 (8) (2006) J87.
[6] R. Haugsrud, T. Norby, J. Am. Ceram. Soc. 90 (4) (2007) 1116.
[7] A.D. Brandao, I. Antunes, J.R. Frade, J. Torre, V.V. Kharton, D.P. Fagg, Chem. Mater. 22 (24) (2010) 6673.
[8] J.P. Bastide, J. Solid State Chem. 71 (1987) 115.
[9] F.J. Manjón, D. Errandonea, J. López-Solano, P. Rodríguez-Hernández, S. Radescu, A. Mujica, A. Muñoz, N. Garro, J. Pellicer-Porres, A. Segura, Ch Ferrer-Roca, R.S. Kumar, O. Tschauner, G. Aquilanti, Phys. Status Solidi (b) 244 (1) (2007) 295.
[10] J.E. Bauerle, J. Phys. Chem. Solids 30 (1969) 2657.
[11] S.M. Haile, G. Staneff, K.H. Ryu, J. Mater. Sci. 36 (2001) 1149.
[12] A.T. Aldred, Mater. Lett. 1 (5,6) (1983) 197.
[13] C. Zheng, A.R. West, Br. Ceram. Trans. J. 89 (1990) 138.
[14] Y.P. Udalov, V.I. Strakhov, O.V. Mel'nikova, O.V. Karpinskaya, M. Dib, A.P. Pivovarova, Russian J. Inorg. Chem. 41 (2) (1996) 292.
[15] G.C. Mather, C.A.J. Fisher, M.S. Islam, Chem. Mater. 22 (21) (2010) 5912.
[16] E. Kendrick, M.S. Islam, P.R. Slater, J. Mater. Chem. 17 (2007) 3104.
[17] D.L. Bish, S.A. Howard, J. Appl. Cryst. 21 (1998) 86.
[18] H. Fjeld, D.M. Kepaptsoglou, R. Haugsrud, T. Norby, Solid State Ionics 181 (2010) 104.
[19] T. Mokkelbost, H.L. Lein, P.E. Vullum, R. Holmestad, T. Grande, M.-A. Einarsrud, Ceram. Int. l (35) (2009) 2877–2883.